

## Versatile Fe–Sn Bonding Interactions in a Metallostannylene System: Multiple Bonding and C–H Bond Activation

Rex C. Handford, Mark A. Nesbit, Patrick W. Smith, R. David Britt, and T. Don Tilley\*

Cite This: *J. Am. Chem. Soc.* 2022, 144, 358–367

Read Online

ACCESS |



Metrics &amp; More

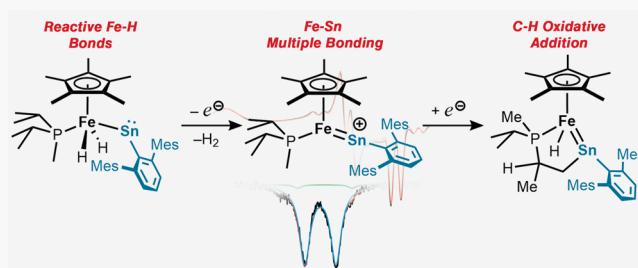


Article Recommendations



Supporting Information

**ABSTRACT:** The metallostannylene  $\text{Cp}^*(\text{Pr}_2\text{MeP})(\text{H})_2\text{Fe-SnDMP}$  (**1**;  $\text{Cp}^* = \eta^5\text{-C}_5\text{Me}_5$ ;  $\text{DMP} = 2,6\text{-dimesitylphenyl}$ ), formed by hydrogen migration in a putative  $\text{Cp}^*(\text{Pr}_2\text{MeP})\text{HFe}[\text{Sn}(\text{H})\text{DMP}]$  intermediate, serves as a robust platform for exploration of transition-metal main-group element bonding and reactivity. Upon one-electron oxidation, **1** expels  $\text{H}_2$  to generate the coordinatively unsaturated  $[\text{Cp}^*(\text{Pr}_2\text{MeP})\text{Fe}=\text{SnDMP}][\text{B}(\text{C}_6\text{F}_5)_4]$  (**3**), which possesses a highly polarized Fe–Sn multiple bond that involves interaction of the tin lone pair with iron. Evidence from EPR and  $^{57}\text{Fe}$  Mössbauer spectroscopy, along with DFT studies, shows that **3** is primarily an iron-based radical with charge localization at tin. Upon reduction of **3**, C–H bond activation of the phosphine ligand was observed to produce  $\text{Cp}^*\text{HFe}(\kappa^2\text{-}(\text{P},\text{Sn})=\text{Sn}(\text{DMP})\text{CH}_2\text{CHMePMe'Pr})$  (**5**). Complex **5** was also accessed via thermolysis of **1**, and kinetics studies of this thermolytic pathway indicate that the reductive elimination of  $\text{H}_2$  from **1** to produce a stannylyne intermediate,  $\text{Cp}^*(\text{Pr}_2\text{MeP})\text{Fe}[\text{SnDMP}]$  (**A**), is likely rate-determining. Evidence indicates that the production of **5** proceeds through a concerted C–H bond activation. DFT investigations suggest that the transition state for this transformation involves C–H cleavage across the Fe–Sn bond and that a related transition state where C–H bond activation occurs exclusively at the tin center is disfavored, illustrating an effect of iron–tin cooperativity in this system.



## INTRODUCTION

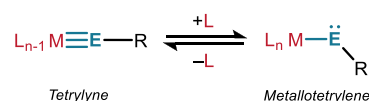
Studies of multiple bonds between a transition metal and a heavy group 14 element provide fundamental insights into chemical bonding and periodic trends.<sup>1–4</sup> Complexes with such M–E bonds give rise to unique transformations that differ significantly from those of analogous species that feature the lightest group 14 element, carbon.<sup>1,3,5,6</sup> Whereas the chemical behavior of metal–carbon double and triple bonds is fairly well understood, the nature of related unsaturated bonds involving more diffuse and higher-energy valence orbitals of the group 14 elements ( $nsnp$ ,  $n > 3$ ) is much less explored.<sup>7</sup> Indeed, the heavier group 14 elements are identified with a strong reluctance to engage in multiple-bond interactions.<sup>8–10</sup>

For mid- to late-transition metal complexes with formally double bonds to silicon (i.e., silylene complexes,  $\text{M} = \text{SiR}_2$ ), charge localization at the silicon atom is a critical factor in determining reactivity patterns.<sup>5,11</sup> For example, cationic group 8 silylene complexes of the type  $[\text{Cp}^*(\text{R}_3\text{P})(\text{H})_2\text{MSiHR}']^+$  ( $\text{Cp}^* = \eta^5\text{-C}_5\text{Me}_5$ ;  $\text{M} = \text{Ru}, \text{Os}$ ) possess little M–Si double-bond character and exhibit strong positive charge localization at silicon, leading to rapid insertions of olefins into the Si–H bond.<sup>12–14</sup> In contrast, the neutral analogues  $\text{Cp}^*(\text{R}_3\text{P})(\text{H})\text{-M}=\text{SiHR}'$  ( $\text{M} = \text{Ru}, \text{Os}$ ) do not react with olefins, even at elevated temperatures.<sup>12</sup>

Although M–E  $\pi$ -bonding character plays a strong role in influencing reactivity, the coordination number at E is also an important factor. In particular, bonding to transition-metal

centers may enforce reactive, low-coordinate structures. This is seen in  $\text{L}_n\text{M}\equiv\text{E-R}$  species that possess a formal triple bond, such as  $\text{Cp}(\text{OC})_2\text{Mo}\equiv\text{Si}(2,6\text{-Trip}_2\text{C}_6\text{H}_3)$  ( $\text{Trip} = 2,4,6\text{-triisopropylphenyl}$ )<sup>15</sup> and  $(\text{Me}_3\text{P})_2(\text{Ph}_3\text{P})\text{Rh}\equiv\text{E}(2,6\text{-Trip}_2\text{C}_6\text{H}_3)$  ( $\text{E} = \text{Sn}, \text{Pb}$ ),<sup>16</sup> which exhibit a linear geometry at E (Scheme 1, left). Related structures that may be viewed as having a single M–E bond possess bent geometries as expected for a divalent group 14 compound. These metallotetrylene complexes (Scheme 1, right) possess a stereochemically active lone pair that can participate in Lewis acid–base interactions.<sup>17–19</sup> In principle, this lone pair may engage with the metal to generate a linear tetrylyne structure, as observed in

## Scheme 1. Interconversion of Tetrylyne and Metallotetrylene Complexes



Received: September 24, 2021

Published: December 27, 2021



the conversion of  $\text{Cp}(\text{OC})_3\text{M}-\text{Ge}(2,6\text{-Trip}_2\text{C}_6\text{H}_3)$  to  $\text{Cp}(\text{OC})_2\text{M}\equiv\text{Ge}(2,6\text{-Trip}_2\text{C}_6\text{H}_3)$  by the photochemical or thermal dissociation of CO ( $\text{M} = \text{Cr}, \text{W}$ ).<sup>20</sup>

A goal of research on tetrylene and metallotetrylene complexes is to develop new chemical transformations and catalysis that utilize bond activations by the [MER] fragment. Along these lines, it has been demonstrated that treatment of the osmium silylidyne complex  $[\text{Cp}^*(\text{Pr}_3\text{P})(\text{H})\text{Os}\equiv\text{SiTrip}][\text{HB}(\text{C}_6\text{F}_5)_3]$  with diphenylacetylene or *tert*-butylphosphalkyne results in [2+2] cycloaddition across the Os–Si triple bond, while terminal alkynes undergo C–H bond activation to generate silylene complexes  $[\text{Cp}^*(\text{Pr}_3\text{P})(\text{H})(\text{RC}\equiv\text{C})\text{Os}=\text{Si}(\text{H})\text{Trip}][\text{HB}(\text{C}_6\text{F}_5)_3]$ .<sup>21</sup> Another interesting example is based on the metallogermylene  $[\text{Cp}^*(\text{OC})_3\text{W}-\text{Ge}-\text{IPr}][\text{B}-(3,5\text{-}(\text{F}_3\text{C})_2\text{C}_6\text{H}_3)_4]$  (IPr = 1,3-bis(2,6-diisopropylphenyl)-imidazol-2-ylidene), which inserts into the element–hydrogen bonds of dihydrogen, HBPIn (Pin = pinacolato), and  $\text{HSiMe}_2\text{Et}$  to give products incorporating four-coordinate germanium centers.<sup>22</sup>

Compared to 4d- and 5d-metal complexes, first-row transition-metal species often exhibit weaker and more reactive metal–ligand bonds and more readily possess high-spin ground states that influence reaction pathways.<sup>23–27</sup> Such factors appear to play a role in the properties of iron silylene complexes  $\text{Cp}^*(\text{Pr}_2\text{MeP})\text{HFe}=\text{SiHAr}$  ( $\text{Ar} = \text{Trip}, 2,6\text{-dimesitylphenyl (DMP)}$ ) recently reported by this laboratory.<sup>28</sup> These diamagnetic species are in equilibrium with  $S = 1$  silyl complexes of the form  $\text{Cp}^*(\text{Pr}_2\text{MeP})\text{Fe}-\text{SiH}_2\text{Ar}$  via reversible hydrogen migration and intramolecularly activate aliphatic C–H bonds by addition across the Fe–Si linkage. The related cationic complexes  $[\text{Cp}^*(\text{Pr}_2\text{MeP})\text{H}_2\text{FeSiHAr}]^+$  ( $\text{Ar} = \text{Ph}, p\text{-tolyl}$ ) are also exceptionally active hydrosilylation catalysts.<sup>29</sup>

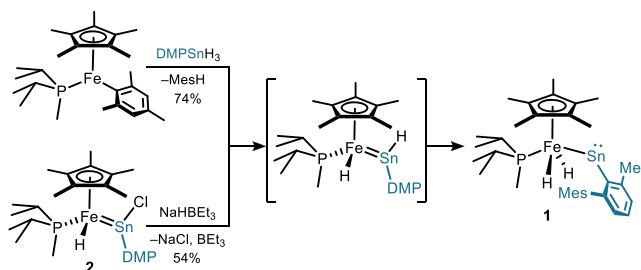
As illustrated in Scheme 1, [MER] linkages are prone to distortions that change the bond order and thus the electron density shared between the M and E centers. In this regard, the tetrylene/metallotetrylene interconversion is similar to the relationship between linear and bent nitrosyl ligands. Nitrosyl ligands have been demonstrated to adaptively change geometry to sequester or release electron density from/to metal centers, in a manner that generates high reactivity.<sup>30–32</sup> In light of the structural connections between metal nitrosyl and [MER] species, a systematic examination of geometry and charge distribution and their effect on bonding and reactivity in [MER] species was sought. Thus, this article describes investigations of novel neutral and monocationic [FeSnR] compounds that span a range of Fe–Sn bond orders. In particular, the ferrostannylene  $\text{Cp}^*(\text{Pr}_2\text{MeP})(\text{H})_2\text{Fe}-\text{SnDMP}$  (**1**) and the stannyne complex  $\text{Cp}^*(\text{Pr}_2\text{MeP})(\text{H})\text{Fe}[\text{Sn}(\text{Cl})\text{DMP}]$  (**2**) provide pathways to cationic complexes possessing unsaturated Fe–Sn bonds, and the putative stannyne  $\text{Cp}^*(\text{Pr}_2\text{MeP})\text{Fe}[\text{SnDMP}]$  (**A**; generated as a reactive intermediate) undergoes spontaneous intramolecular activation of a C–H bond in the phosphine ligand.

## RESULTS AND DISCUSSION

### Ferrostannylene $\text{Cp}^*(\text{Pr}_2\text{MeP})(\text{H})_2\text{Fe}-\text{SnDMP}$ (**1**).

Complex **1** was prepared by addition of  $\text{DMPSnH}_3$  to a solution of  $\text{Cp}^*(\text{Pr}_2\text{MeP})\text{FeMe}$ <sup>28</sup> (Scheme 2). By  $^1\text{H}$  and  $^{31}\text{P}\{^1\text{H}\}$  NMR spectroscopy, **1** and mesitylene are the major products, and workup of the reaction mixture gave analytically pure dark brown blocks of **1** from pentane in good yield (74%). The room-temperature  $^1\text{H}$  NMR spectrum of **1** in

### Scheme 2. Synthetic Routes Leading to Complex 1



benzene-*d*<sub>6</sub> displays a single hydride resonance at  $\delta -17.1$  ppm, consistent with  $C_s$  symmetry in solution. This signal exhibits characteristic satellites due to the nearby tin nucleus ( $^2J_{\text{SnH}}$  242.9 Hz;  $^{119}\text{Sn}\{^1\text{H}\}$  NMR:  $\delta_{\text{Sn}}$  2515 ppm), and the coupling constant is similar in magnitude to those observed in other hydridometallostannylene complexes.<sup>19,33</sup> X-ray diffraction analysis of a single crystal of **1** (Figure 1a) reveals an Fe–Sn

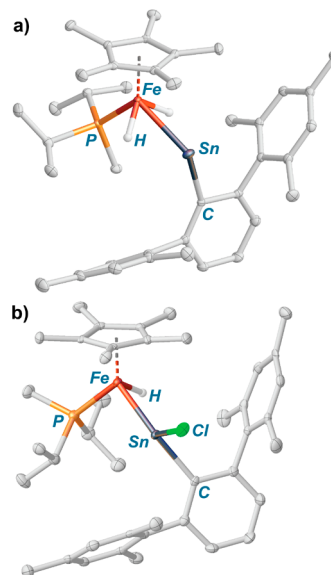


**Figure 1.** Solid-state molecular structures of **1** (a) and **2** (b) with 50% probability thermal ellipsoids drawn.

distance of 2.5739(5) Å and elongated Sn–H distances (2.18(2), 2.11(3) Å) that are in accord with weak Sn...H interactions.<sup>34</sup> The zero-field  $^{57}\text{Fe}$  Mössbauer spectrum of a frozen (80 K) toluene solution of **1** (Figure 4a) displays a quadrupole doublet ( $\delta = -0.211$  mm  $\text{s}^{-1}$ ,  $\Delta E_q = 1.649$  mm  $\text{s}^{-1}$ ) with an isomer shift corresponding to the negative extreme of the range typically spanned by  $S = 0$  Fe(II) complexes.<sup>35</sup> Although the utility of the oxidation state formalism<sup>36,37</sup> is limited by the prevalence of covalent bonding in **1**, the isomer shift of **1** relative to its closely related cationic derivatives (i.e., **3**, **4**; *vide infra*) indicates that it is best described as an Fe(II) complex.

By analogy with the congeneric ruthenium systems  $\text{Cp}^*(\text{Pr}_2\text{MeP})(\text{H})_2\text{Ru}-\text{SnDMP}$ <sup>19</sup> and  $\text{Cp}^*(\text{IXy})(\text{H})_2\text{Ru}-\text{SnTrip}$  ( $\text{IXy} = 1,3\text{-bis-xylyl-imidazol-2-ylidene}$ ),<sup>33</sup> the formation of **1** presumably occurs via a stannyne tautomer,  $\text{Cp}^*(\text{Pr}_2\text{MeP})\text{HFe}[\text{Sn}(\text{H})\text{DMP}]$ , although in this case complete conversion to the metallotstannyne (**1**) occurred in less than 5 min under ambient conditions, and an intermediate stannyne complex was not observed by  $^1\text{H}$  or  $^{31}\text{P}\{^1\text{H}\}$  NMR spectroscopy

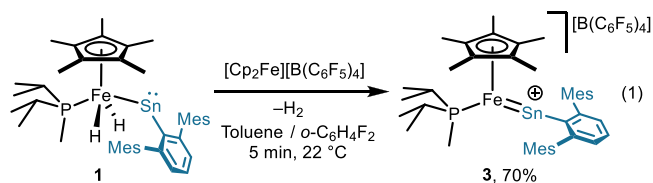
(benzene- $d_6$ ). The intermediacy of  $\text{Cp}^*(\text{Pr}_2\text{MeP})\text{HFe}[\text{Sn}(\text{H})\text{DMP}]$  is further implied by the fact that **1** can also be prepared by treatment of the chlorostannylene complex  $\text{Cp}^*(\text{Pr}_2\text{MeP})\text{HFe}[\text{Sn}(\text{Cl})\text{DMP}]$  (**2**) with  $\text{NaHBET}_3$  (Scheme 2). Complex **2** was prepared by treatment of  $\text{Cp}^*(\text{Pr}_2\text{MeP})\text{HFe}(\text{N}_2)$  with 0.5 equiv of  $[\text{DMP}(\text{SnCl})_2]$ . In the single-crystal solid-state molecular structure of **2** (Figure 1b), the Fe–Sn distance (2.3891(7) Å; averaged between two molecules in the asymmetric unit) is contracted by nearly 0.2 Å compared to that in **1**.

Compared to **1**, the  $^1\text{H}$  NMR spectrum of **2** displays a hydride resonance that exhibits a larger coupling constant to tin ( $\delta$  –14.4 ppm;  $d$ ,  $^2J_{\text{HP}}$  63.3 Hz,  $^2J_{\text{HSn}}$  472.7 Hz), while the tin chemical shift in the  $^{119}\text{Sn}\{^1\text{H}\}$  NMR spectrum of **2** is substantially more upfield ( $\delta_{\text{Sn}}$  582 ppm). Variable-temperature  $^1\text{H}$  NMR spectra of **2** in toluene- $d_8$  reveal a decoalescence process beginning at 240 K and the resolution of two species at 210 K in a relative ratio of 81:19. The major and minor species are presumed to be stereoisomers, as they are generated by decoalescence from a common parent species and are presumably interconverted by rotations about the Fe–Sn– $\text{C}_{\text{ipso}}$  linkage. Furthermore, the  $^1\text{H}$  and  $^{31}\text{P}\{^1\text{H}\}$  NMR spectroscopic features of the major species are in accord with those expected based on the solid-state structure of **2**. These observations are similar to those previously reported for the ruthenium congener of **2**,  $\text{Cp}^*(\text{Pr}_2\text{MeP})\text{HRu}[\text{Sn}(\text{Cl})\text{DMP}]$  (**2**<sub>Ru</sub>).<sup>19</sup> Consistently, the zero-field  $^{57}\text{Fe}$  Mössbauer spectrum of **2** at 80 K (Supporting Information Figure S12) possesses two quadrupole doublets with  $\delta$ ,  $\Delta E_{\text{q}}$  (mm  $\text{s}^{-1}$ ) = –0.254, 2.066 (76% relative area) and –0.189, 2.495 (24% relative area). The similarity of these isomer shifts to that of **1** suggests that these complexes possess comparable charge densities at the formally Fe(II) centers. The increased quadrupole splittings relative to **1** are a manifestation of the reduced symmetry about the iron center in **2**.

Compound **1** is unique among 3d-metal metallostanlylenes in that it possesses hydride ligands as potential reaction centers; for example, H–H reductive elimination should create a coordinatively unsaturated iron center. Other comparable species such as  $\text{Cp}(\text{OC})_3\text{Cr}\text{--}\text{SnDMP}$ ,<sup>38</sup>  $\text{Cp}(\text{OC})_2\text{Fe}\text{--}\text{SnAr}$ ,<sup>39</sup> and  $[\text{Cp}(\text{OC})\text{Fe}(\text{SnAr})_2]$ <sup>39</sup> possess strongly coordinated ancillary ligands expected to be relatively nonlabile under nonphotolytic conditions. Thus, the reaction chemistry associated with **1** was examined to explore the nature of the Fe–Sn bond as well as to provide access to coordinatively unsaturated analogues.

**Cationic Complexes Possessing Fe–Sn Multiple Bonding.** The oxidation of **1** was examined as a means to induce electronic unsaturation at the iron center and enable  $\text{Sn} \rightarrow \text{Fe}$   $\pi$ -donation. A complementary thermolytic pathway that induces  $\text{H}_2$  elimination in **1** to generate a transient, unsaturated Fe–Sn species was also explored (*vide infra*). Complex **1** was treated with  $[\text{Cp}_2\text{Fe}][\text{B}(\text{C}_6\text{F}_5)_4]$  in a mixture of toluene and 1,2-difluorobenzene, resulting in a rapid color change from dark brown to greenish-orange;  $^1\text{H}$  NMR spectroscopic analysis of the product mixture (as a 25% v/v 1,2-difluorobenzene/benzene- $d_6$  solution) indicated the formation of ferrocene,  $\text{H}_2$ , and a new paramagnetic product (**3**).

Following trituration with pentane, crystallization of the paramagnetic product by pentane diffusion into a saturated 1,2-difluorobenzene solution gave large crystalline rods of  $[\text{Cp}^*(\text{Pr}_2\text{MeP})\text{Fe}=\text{SnDMP}][\text{B}(\text{C}_6\text{F}_5)_4]$  (**3**, eq 1). Several features of the crystallographically determined solid-state



molecular structure of **3** (Figure 2) are remarkable. The Fe–Sn bond distance of 2.2889(6) Å is approximately 0.3 and 0.1 Å shorter than the corresponding bonds in **1** and **2**, respectively, and the Fe–Sn– $\text{C}_{\text{ipso}}$  unit is essentially linear ( $\angle = 169.85(9)^\circ$ ). The Fe–Sn bond length is also the shortest 3d-metal–tin distance reported to date (cf.  $[(\text{dmp})_2\text{HMn} \equiv \text{SnDMP}]^+$ ,  $d_{\text{MnSn}} = 2.3434(5)$  Å).<sup>40</sup> Notably, the structural model of **3** exhibits residual electron density near the tin atom, which can be modeled as a second tin site with relative occupancies of 0.94:0.06 using free variables. This minor-component tin atom corresponds to a trace impurity of  $[\text{Cp}^*(\text{Pr}_2\text{MeP})(\text{H})\text{Fe}=\text{SnDMP}][\text{B}(\text{C}_6\text{F}_5)_4]$  (**4**), which was independently synthesized as described later (*vide infra*).

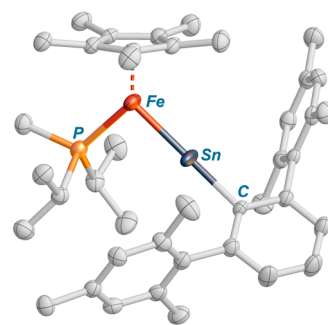


**Figure 2.** Solid-state molecular structure of the cationic portion of **3** with 50% probability thermal ellipsoids drawn.

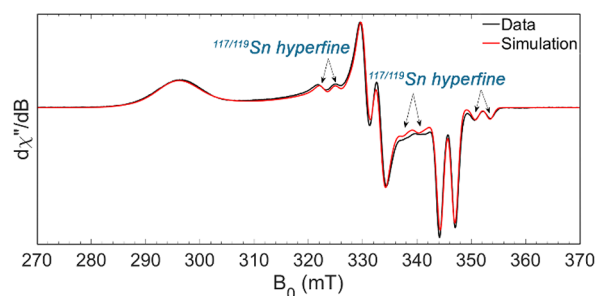


**Figure 3.** X-band ( $\sim 9.69$  GHz) CW EPR spectrum of **3** at 10 K in 2-methyltetrahydrofuran. Microwave power, 0.2 mW; modulation amplitude, 0.5 mT; modulation frequency, 100 kHz; conversion time, 60 ms. Experimental data are shown in black; simulated spectrum are shown in red.

Since the solid-state metrical parameters suggest Fe–Sn multiple bonding in **3**, the electronic structure of this complex was investigated to help reveal the nature of the Fe–Sn interaction. An Evans' method measurement of **3** reveals a solution magnetic moment of 1.8  $\mu_{\text{B}}$ , consistent with an  $S = 1/2$  ground state. Since the unpaired spin may reside on either iron or tin, or be delocalize across both atoms, EPR studies of **3** were undertaken to differentiate between these possibilities. The EPR spectrum of a 2-methyltetrahydrofuran glass of **3** (5 mM) at 10 K contains a rhombic signal with  $g = 2.3414$ , 2.0873, and 2.0044 ( $g_{\text{iso}} = 2.1444$ ), showing resolved hyperfine



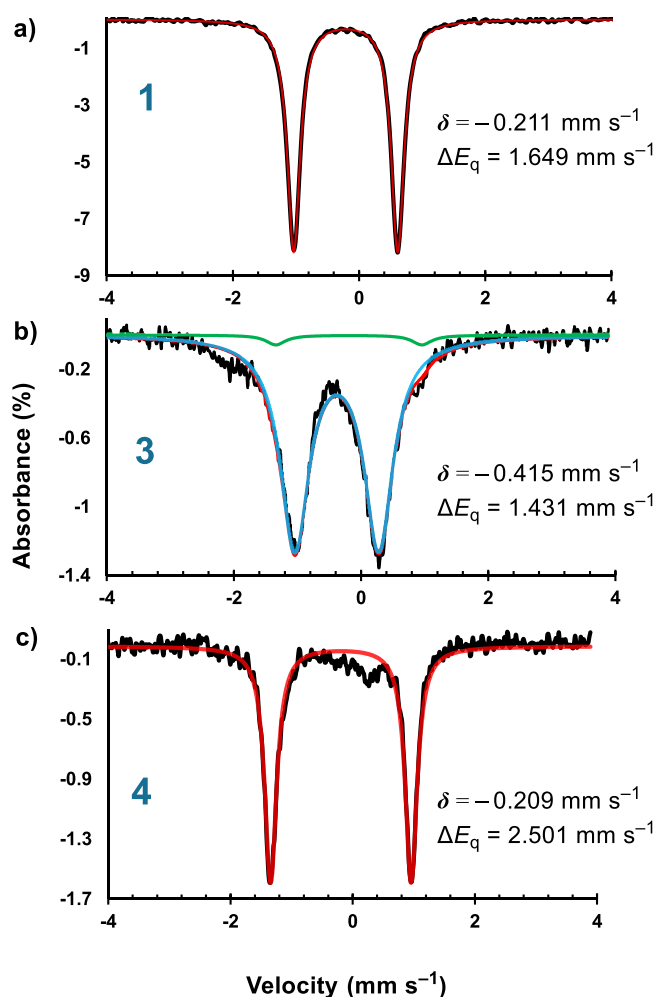


**Figure 4.** Zero-field  $^{57}\text{Fe}$  Mössbauer spectra of natural abundance frozen solutions (80 K) of (a) 1 in toluene, (b) 3 in 1,2-difluorobenzene showing the presence of trace quantities of 4 (green trace), and (c) 4 in 1,2-difluorobenzene. Data are presented in black traces, and simulations are presented in colored traces.

coupling to  $^{31}\text{P}$  and  $^{117/119}\text{Sn}$  at mid- and high-field  $g$  values (Figure 3). The value of  $g_{\text{iso}}$  indicates that the radical is Fe centered,<sup>41–48</sup> and the magnitudes of the relatively small hyperfine couplings to both  $^{31}\text{P}$  ( $a_{\text{iso}} = 77.3 \text{ MHz}$ )<sup>49–52</sup> and  $^{117/119}\text{Sn}$  ( $a_{\text{iso}} = 439 \text{ MHz}$  for  $^{119}\text{Sn}$ , cf.  $\sim 1700 \text{ MHz}$  for tin-localized radicals<sup>47,48</sup>) are consistent with this interpretation.

$^{57}\text{Fe}$  Mössbauer studies were undertaken to experimentally characterize the charge distribution in 3. The zero-field spectrum of a frozen 1,2-difluorobenzene solution of 3 at 80 K (Figure 4b) exhibits a quadrupole doublet centered at a low isomer shift ( $\delta = -0.415 \text{ mm s}^{-1}$ ) with a large quadrupole splitting ( $\Delta E_q = 1.431 \text{ mm s}^{-1}$ ). The isomer shift is somewhat more negative than that of the range spanned by other  $S = 1/2$  Fe(III) complexes,<sup>35,53,54</sup> a feature that can be understood in terms of the strongly donating, highly covalent ligand sphere of 3. In line with this interpretation is the large quadrupole splitting observed for 3, which reflects significant involvement of the iron 4s orbital in bonding. The  $^{57}\text{Fe}$  Mössbauer spectrum of 3 indicates the presence of a minor, second species (4), whose quadrupole doublet was modeled with a 3% relative area using fitting parameters obtained from an authentic sample of 4 (*vide infra*). These observations are consistent

with the presence of small quantities of cocrystallized 4 in the solid-state molecular structure of 3.

Restricted open-shell DFT calculations (see Supporting Information page S20 for details) of complex 3, at the  $\omega\text{B97X-D3}^{55}/\text{def2-SVP}(\text{C,H}),\text{def2-TZVP}(\text{Fe,Sn,P})^{56}$  level of theory, reproduces the geometry of 3 in the solid state with good accuracy (Figure 5a,  $d(\text{Fe}–\text{Sn}) = 2.29 \text{ \AA}$ ,  $\angle(\text{Fe}–\text{Sn}–\text{C}_{\text{ipso}}) =$

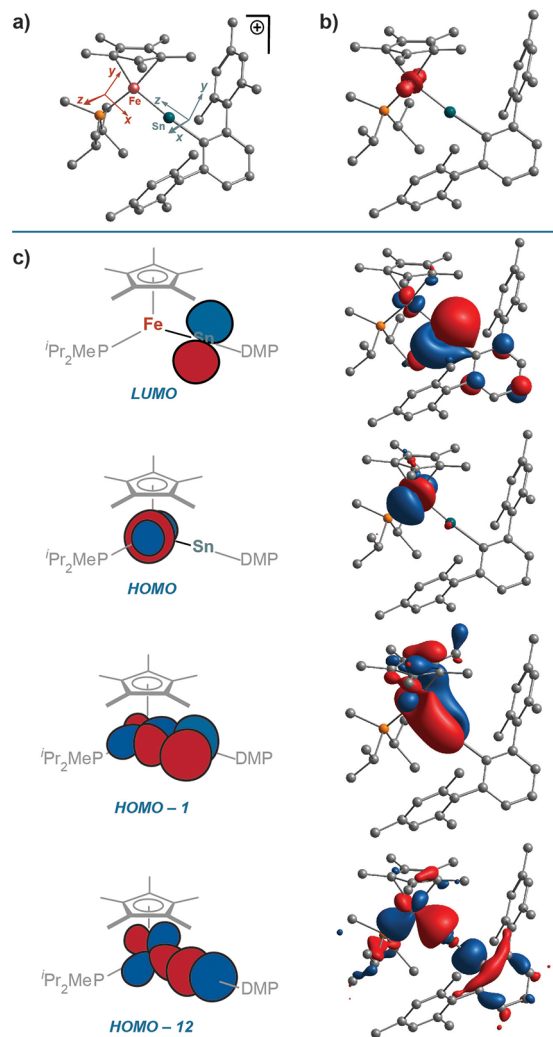


**Figure 5.** (a) Optimized structure of 3 and coordinate axes defined for iron and tin atoms. (b) Spin-density plot of 3 at an isovalue of 0.03. (c) Left column: simplified depiction of MOs; right column: rendering of MOs at an isovalue of 0.04.

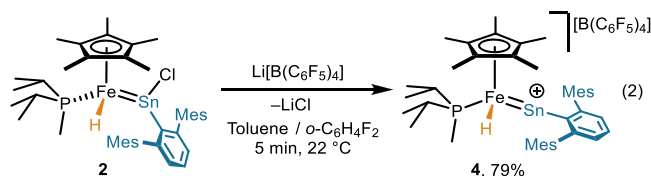
$175.19^\circ$ ). The spin-density plot of 3 indicates that the unpaired spin is primarily localized on iron (Figure 5b), which is consistent with the calculated natural spin densities ( $S_{\text{Fe}} = 0.82$ ,  $S_{\text{Sn}} = 0.05$ ) and natural charges ( $q_{\text{Fe}} = -0.27$ ,  $q_{\text{Sn}} = 1.69$ ). In electron counting terms, 3 is a 17-electron complex in which the  $[\text{SnDMP}]$  fragment functions as an LX-type ligand (donating three electrons) that interacts with iron through  $\sigma$ - and  $\pi$ -bonding interactions. Two lines are drawn between the tin and iron centers to represent these two bonding interactions, although three electrons are donated to iron overall. The observed bent and linear coordination modes for the  $[\text{SnDMP}]$  ligand (in 1 and 3, respectively) are therefore reminiscent of the behavior of nitrosyl (NO) ligands, which similarly behave as one- and three-electron ligands depending

on the electronic requirements of the metal-based fragment.<sup>32,57,58</sup>

**Table 1.** Summary of Calculated and Experimental Parameters for Fe–Sn Bonds

species	WBI	$d(\text{Fe–Sn})_{\text{calc}}$ , Å	$d(\text{Fe–Sn})_{\text{exp}}$ , Å
1	0.97	2.57	2.5739(5)
2	1.30	2.41	2.3891(7)
3	1.86	2.29	2.2889(6)
4	1.40	2.34	2.2879(7)
A	1.78	2.30	

Inspection of the canonical molecular orbitals (MOs) calculated by DFT (Figure 5c) shows that the HOMO/SOMO of **3** is  $\text{Fe}(3d_z^2)$  based, while the LUMO is  $\text{Sn}(5p)$  in character. The Fe–Sn  $\pi$ - and  $\sigma$ -bonds arise from  $\text{Fe}(3d)$ – $\text{Sn}(5p)$  orbital interactions in HOMO–1 and HOMO–12, respectively, defining an Fe–Sn double bond. The Fe–Sn Wiberg bond index<sup>59</sup> (WBI) of **3** (1.86) is significantly greater than those computed for **1** (0.97) and **2** (1.30), indicating increased bond order in the cation (relevant parameters are summarized in Table 1). This marked increase in bond order presumably reflects greater Coulombic attraction in **3** resulting from extensive charge transfer from tin to iron; this is further supported by the calculated natural charges on the iron and tin atoms of **3** (*vide supra*).



During these investigations, it was noted that many preparations of **3** included a second minor product (**4**), whose  $^1\text{H}$  NMR spectroscopic features point to a diamagnetic iron monohydride species ( $\delta = 13.6$  ppm, which integrates to 1H relative to  $\text{Cp}^*$ ). Although this species is generally present only in trace quantities, it is formed in significantly greater amounts (up to 25%) in the presence of adventitious THF. Given the possibility that this species is the corresponding H atom adduct of **3**, namely,  $[\text{Cp}^*(\text{Pr}_2\text{MeP})(\text{H})\text{Fe}=\text{SnDMP}][\text{B}(\text{C}_6\text{F}_5)_4]$  (**4**), a deliberate synthetic route was sought. Abstraction of chloride from **2** by treatment with  $\text{Li}[\text{B}(\text{C}_6\text{F}_5)_4]$  in 1,2-difluorobenzene solution resulted in the formation of greenish-brown **4** in 79% yield. The  $^1\text{H}$  NMR spectrum of an authentic sample of **4** is identical with that observed for the diamagnetic product found in certain preparations of **3**, with  $^2J_{\text{SnH}}$  325.7 Hz and  $\delta_{\text{Sn}}$  1027 ppm. The crystallographically determined solid-state molecular structure of **4** (Figure 6) reveals an additional hydride ligand that was located in the Fourier difference map and refined isotropically. The structural model of **4** exhibits disorder of the tin atom across two sites with relative occupancies of 0.74 and 0.26, with the major component having the metrical parameters  $\angle(\text{Fe–Sn–C}_{\text{ipso}}) = 157.57(7)^\circ$  and  $d(\text{Fe–Sn}) = 2.2879(7)$  Å; the related parameters for the minor disordered component are similar. Compared to **3**, the Fe–Sn bond length is essentially unchanged, but the Fe–Sn– $\text{C}_{\text{ipso}}$  linkage is significantly more bent. This structural distortion likely arises from the increased coordination number of iron in **4**.

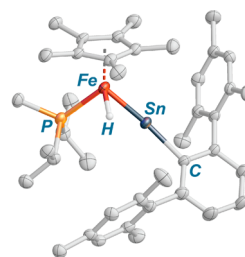
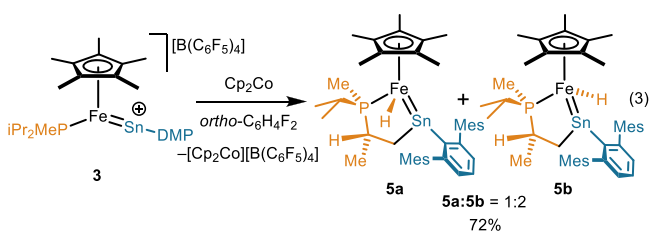


**Figure 6.** Solid-state molecular structure of the cationic portion of **4** with 50% probability thermal ellipsoids drawn.

The zero-field  $^{57}\text{Fe}$  Mössbauer spectrum of an 80 K 1,2-difluorobenzene glass of **4** reveals a quadrupole doublet (Figure 4c) centered at  $-0.209$  mm  $\text{s}^{-1}$  with  $\Delta E_{\text{q}} = 2.501$  mm  $\text{s}^{-1}$ . The isomer shift for **4** is nearly identical with that of **1**, indicating similar charge densities at both iron centers and suggesting that the H atom in **4** may have a reducing effect on iron (i.e., that the “hydride” ligand may possess protic character). The diminished symmetry about the iron center in **4** is manifest in the significantly greater quadrupole splitting compared to those of **1** or **3**. In terms of Fe–Sn bonding, **4** is similar to **3**; a natural population analysis of the cationic portion of **4** shows that the positive charge in this species is similarly localized at tin ( $q_{\text{Fe}} = -0.34$ ,  $q_{\text{Sn}} = +1.60$ ), and the Fe–Sn WBI of 1.40 is in between those of **2** and **3**.

**Intramolecular C–H Bond Activation at Tin.** Given the formal 17-valence-electron configuration for **3**, investigation of its one-electron reduction was of interest. Treatment of **3** with 1 equiv of  $\text{Cp}_2\text{Co}$  in a 25% v/v 1,2-difluorobenzene/benzene- $d_6$  mixture resulted in rapid formation of a deep purple solution and a single new diamagnetic species (**5a**, by  $^1\text{H}$  NMR spectroscopy). In solution, **5a** gradually diminished in concentration to become the minor component of a two-component mixture containing another species (**5b**); the equilibrium **5a**:**5b** ratio came to 1:2. Both **5a** and **5b** possess Fe–H, phosphine, and Sn-containing moieties, as evidenced by their characteristic  $^1\text{H}$  NMR resonances occurring at  $\delta = 16.1$  ppm (d,  $^2J_{\text{HP}}$  43.1 Hz,  $^2J_{\text{HSn}}$  276 Hz) and  $\delta = 15.8$  ppm (d,  $^2J_{\text{HP}}$  62.6 Hz,  $^2J_{\text{HSn}}$  296 Hz), respectively. The  $^{119}\text{Sn}\{^1\text{H}\}$  NMR spectrum of the mixture exhibits two resonances at  $\delta$  1009 ppm (d,  $^2J_{\text{SnP}}$  221 Hz; **5a**) and 1081 ppm (d,  $^2J_{\text{SnP}}$  231 Hz; **5b**) in a 1:2 ratio.

Cooling of an ether/ $(\text{Me}_3\text{Si})_2\text{O}$  solution of the crude reaction mixture resulted in formation of purple blocks that were revealed by single-crystal X-ray diffraction analysis to be the C–H bond activation product  $\text{Cp}^*\text{HFe}(\kappa^2\text{-(P,Sn)})=\text{Sn}(\text{DMP})\text{CH}_2\text{CHMePMe}^i\text{Pr}$  (stereochemistry corresponding to **5b**, Figure 7; see below). A combination of  $^1\text{H}$  NMR, nuclear Overhauser effect spectroscopy (NOESY), and COSY experiments on the **5a,b** mixture in benzene- $d_6$  indicated that these species differ only in the orientation of the hydride ligand and that these complexes are diastereomers (stereochemistry is shown in eq 3). The solution-state characterization of **5b** is



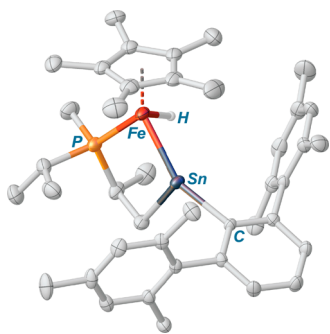


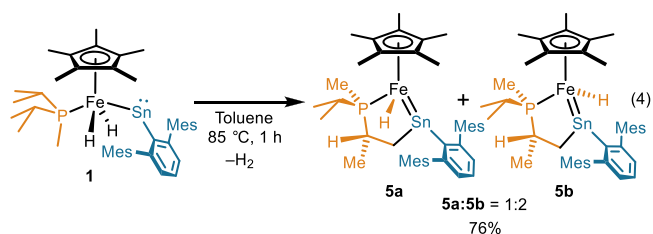
**Figure 7.** Solid-state molecular structure of **5b** with 50% probability thermal ellipsoids drawn.

fully consistent with its solid-state molecular structure. The zero-field  $^{57}\text{Fe}$  Mössbauer spectrum of a frozen toluene glass of **5a,b** (80 K) shows two quadrupole doublets with relative areas of ca. 72% and 28%, which were fitted with parameters  $\delta$ ,  $\Delta E_q$  ( $\text{mm s}^{-1}$ ) =  $-0.223$ ,  $1.890$  and  $-0.209$ ,  $2.403$ , respectively (see [Supporting Information](#) page S18). These isomer shifts are similar to those of **1** and **4**, indicating that **5a,b** are also best described as Fe(II) complexes.

Presumably, the one-electron reduction of **3** initially produces an intermediate with the formula  $\text{Cp}^*(\text{Pr}_2\text{MeP})\text{Fe}[\text{SnDMP}]$  (**A**), which then transforms to **5a**. In an attempt to observe **A**, the  $\text{Cp}_2\text{Co}$  reduction of **3** in a 25% v/v 1,2-difluorobenzene/toluene- $d_8$  gel at  $-35^\circ\text{C}$  was monitored by  $^1\text{H}$  and  $^{31}\text{P}\{^1\text{H}\}$  NMR spectroscopy. Under these conditions, a major diamagnetic species is produced, displaying well-defined resonances attributed to  $\text{Cp}^*$  ( $\delta_{\text{H}}$  1.22 ppm, 15 H), DMP, and  $\text{Pr}_2\text{MeP}$  ( $\delta_{\text{P}}$  40.6 ppm) moieties in NMR spectra at 258 K. Examination of the  $^1\text{H}$ – $^{31}\text{P}$  HMBC NMR spectrum indicates that this species does not possess a hydride ligand, supporting its assignment as **A**. Upon warming to room temperature, **A** is converted to **5a**, with subsequent isomerization to **5b** occurring over several hours. Repeated attempts to obtain a suitable  $^{119}\text{Sn}\{^1\text{H}\}$  NMR spectrum of **A** were unsuccessful.

The DFT-calculated molecular structure of **A** was geometrically optimized by adaptation from the solid-state molecular structure of **3**. The structure of **A** exhibits a somewhat bent Fe–Sn– $\text{C}_{\text{ipso}}$  bond angle ( $\angle = 169.85^\circ$ ) and a short Fe–Sn bond distance of 2.30 Å. The Fe–Sn WBI for **A** (1.78) is similar to that of **3**, while the natural charges on iron ( $q_{\text{Fe}} = -0.41$ ) and tin ( $q_{\text{Sn}} = 1.02$ ) indicate greater electron density at both atoms. The Fe–Sn bonding in **A** is similar to that in **3** and **4**, with the  $[\text{SnAr}]$  fragment acting as a net three-electron (LX-type) donor through one  $\sigma$  and one  $\pi$  interaction (see [Supporting Information](#) page S25). These computational investigations suggest that the greater accumulation of electron density at the iron and tin centers of **A** facilitates the subsequent C–H bond activation. The lack of related reactivity from **3** or **4** can therefore be viewed as a consequence of the electron-deficient tin centers in these molecules.

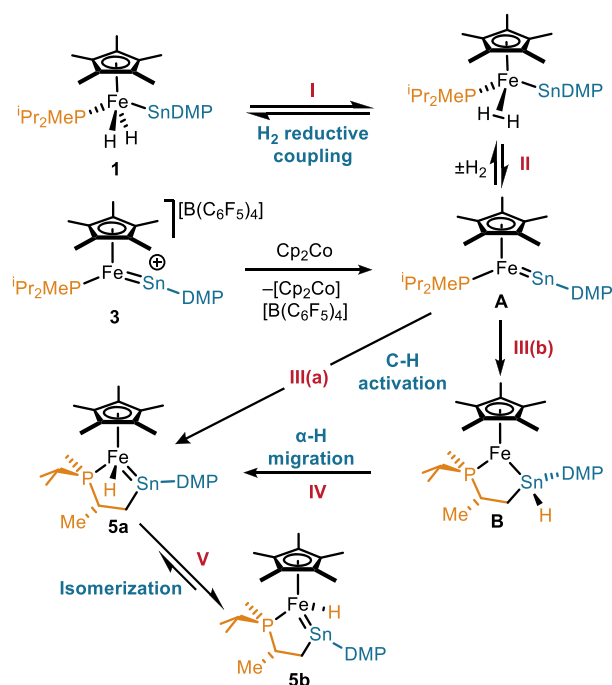
Since the proposed intermediate in the C–H bond activation process (**A**) is closely related to complex **1**, a direct synthesis of **5a,b** from **1** was sought. Indeed, thermolysis of a toluene solution of **1** at  $85^\circ\text{C}$  for 1 h resulted in evolution of  $\text{H}_2$  (by  $^1\text{H}$  NMR spectroscopy) and formation of **5a,b** in a 1:2 ratio as the sole products of the reaction in good yield (76% isolated yield; eq 4). Because activations of aliphatic C–H bonds by tin compounds is uncommon, a mechanistic investigation of this reaction was undertaken.



Potential mechanistic pathways are given in [Scheme 3](#). This process is initiated by reductive coupling and dissociation of  $\text{H}_2$  from **1** (steps I and II) to generate intermediate **A**, which is alternatively produced by reduction of **3**. The proposed elementary steps following  $\text{H}_2$  elimination from **1** involve C–H cleavage by three potential routes: activation of the C–H bond across the Fe–Sn linkage to directly produce **5a** (III(a)) or activation of the C–H bond at tin (III(b)) to produce a stannyl intermediate (**B**), which is converted to **5a** by  $\alpha$ -H migration from tin to iron. Finally, an additional mechanism for the C–H bond activation step could involve oxidative addition at the iron center exclusively. This latter mechanism is unlikely given the steric crowding about the iron center and due to the strain required to generate a hypothetical intermediate of iron-based C–H oxidative addition, the alkyl-hydrido complex  $\text{Cp}^*(\kappa^2-(\text{P},\text{C})\text{-}i\text{PrMePCHMeCH}_2)\text{HFe}[\text{SnDMP}]$ . Indeed, attempts to minimize a model of this intermediate with modestly truncated phosphine and terphenyl ligands,  $\text{Cp}^*(\kappa^2-(\text{P},\text{C})\text{-Me}_2\text{PCHMeCH}_2)\text{HFe}[\text{SnTer}]$ , resulted in its collapse to  $\text{Cp}^*\text{HFe}(\kappa^2-(\text{P},\text{Sn})=\text{Sn}(\text{Ter})\text{-CH}_2\text{CHMePMe}_2)$  (**5a\***).

DFT investigations ( $\omega\text{B97X-D3}^{55}/\text{def2-SVP}(\text{C},\text{H}),\text{def2-TZVP}(\text{Fe},\text{Sn},\text{P})/\text{IEF-PCM}^{60}(\text{benzene})$ ;<sup>61</sup> see [Supporting Information](#) page S20) of the C–H bond activation mechanism were initiated from a truncated model of complex **A**,  $\text{Cp}^*(i\text{PrMe}_2\text{P})\text{Fe}[\text{SnTer}]$  (**A\***). The metrical parameters of

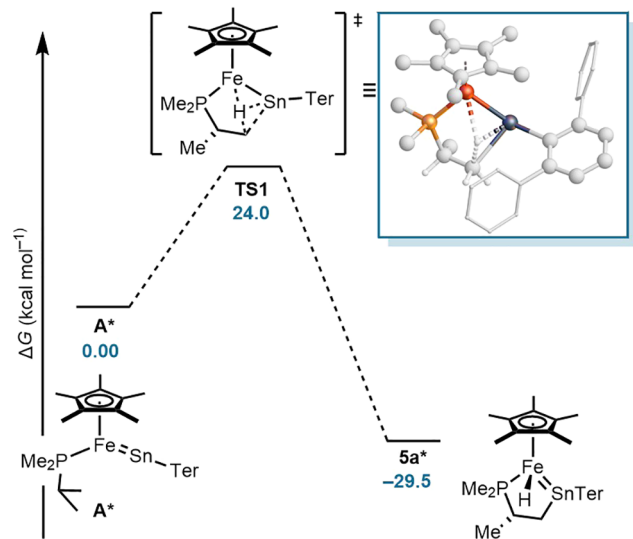
**Scheme 3.** Proposed Mechanisms for the Formation of **5a,b** from **1** or **3**





$A^*$  ( $d(\text{Fe-Sn}) = 2.30 \text{ \AA}$ ,  $\angle(\text{Fe-Sn-C}_{\text{ipso}}) = 157.93^\circ$ ) are broadly similar to those of **A**, although the Fe-Sn-C<sub>ipso</sub> bond angle is moderately more bent; the WBI of  $A^*$  (1.76) is also largely unchanged compared to that of **A**. A freezing string method search<sup>62</sup> located a transition state (**TS1**) corresponding to route III(a) (C-H bond activation across the Fe-Sn bond). The barrier for this transformation—determined by coupled-cluster single-point calculations (DLPNO-CCSD(T)<sup>63</sup>//def2-TZVPP<sup>56</sup>/CPCM<sup>64</sup> (benzene);<sup>61</sup> see [Supporting Information](#) page S20)—is  $\Delta G^\ddagger_{298 \text{ K}} = 24.0 \text{ kcal mol}^{-1}$ , and the overall transformation to  $\text{Cp}^*\text{HFe}(\kappa^2\text{-}(\text{P},\text{Sn})=\text{Sn}(\text{Ter})\text{-CH}_2\text{CHMePMe}_2)$  (**5a**<sup>\*</sup>) is exothermic with  $\Delta G_{298 \text{ K}} = -29.5 \text{ kcal mol}^{-1}$  ([Scheme 4](#)). Although the calculated barrier is

**Scheme 4. Calculated Reaction Profile for C-H Bond Activation across the Fe-Sn Linkage<sup>a</sup>**



<sup>a</sup>Inset: optimized structure of **TS1**. Most hydrogen atoms have been omitted for clarity.

greater than expected based on a qualitative examination of the reaction rate when **5a** is generated via reduction of **3**, this model nonetheless provides a plausible mechanism for the C-H bond activation. Compared to  $A^*$ , the structure of **TS1** exhibits a similar Fe-Sn-C<sub>ipso</sub> bond angle ( $\angle = 152.95^\circ$ ) but possesses a lengthened Fe-Sn bond ( $d = 2.54 \text{ \AA}$ ). As well, the extent of Fe-Sn multiple bonding in **TS1** is substantially reduced relative to  $A^*$ , as evidenced by the WBI (1.09), which is comparable to metallostannylene **1**. The natural charge of the tin atom in **TS1** ( $q_{\text{Sn}} = 0.62$ ) is also diminished relative to that of  $A^*$ . Additionally, the iron and tin atoms both engage in interactions with the hydrogen atom of the C-H bond ( $d(\text{Fe-H}) = 2.21$ ,  $d(\text{Sn-H}) = 1.87$ ).

The HOMO of **TS1** displays an overlap of the Fe-Sn  $\sigma$ -bonding orbital with the C-H antibond,  $\sigma^*(\text{C-H})$  ([Figure 8](#)); this interaction appears to be enhanced by the bent Fe-Sn-C<sub>ipso</sub> linkage, which orients the  $\sigma(\text{Fe-Sn})$  bonding electron density toward the C-H bond. It is likely that the reduction in Fe-Sn bond order of **TS1** plays a crucial role in the transformation: the electron density previously engaged in multiple bonding in  $A^*$  is “released” to the C and H atoms to facilitate the bond-breaking step. DFT investigations further illustrate that C-H bond activation occurring at the tin atom alone without cooperative participation by the iron atom (i.e.,

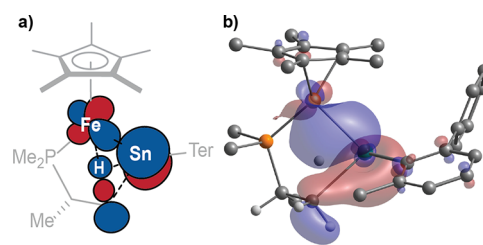


**Figure 8.** (a) Simplified depiction of the HOMO of **TS1**. (b) Rendering of the HOMO of **TS1** at an isovalue of 0.04. The carbon atoms of one phenyl ring—other than C<sub>ipso</sub>—as well as most hydrogen atoms have been hidden for clarity.

process III(b) in [Scheme 3](#)) is significantly less favorable ( $\Delta G^\ddagger_{298 \text{ K}} = 31.6 \text{ kcal mol}^{-1}$ ; see [Supporting Information](#) page S21).

The C-H bond activation reaction was experimentally interrogated by monitoring the thermolysis of **1** at 355 K via <sup>1</sup>H NMR spectroscopy. At concentrations from 5 to 25 mM, the first-order reaction rate constant of  $\sim 1 \times 10^{-3} \text{ s}^{-1}$  slightly decreases with increased concentrations of **1** (see [Supporting Information](#), [Table S1](#)). Complex **5a** and H<sub>2</sub> are the major products at early times in the thermolysis, and **5b** is formed after significant quantities of **5a** are already generated (see [Supporting Information](#) [Figure S3](#)), indicating that **5b** is produced by isomerization of **5a** ([Scheme 3](#), step V). A related isomerization has been observed for  $\text{Cp}^*(\text{iPr}_2\text{MeP})\text{HRu}[\text{Sn}(\text{Cl})\text{DMP}]$  (**2<sub>Ru</sub>**).<sup>19</sup> A plausible mechanism for this interconversion involves dissociation of tin from the iron center of **5a** to transiently generate  $\text{Cp}^*\text{HFe}(\kappa^1\text{-}(\text{P})\text{-Sn}(\text{DMP})\text{-CH}_2\text{CHMePMePr})$ ; movement of the hydride ligand to the other side of the Cp\*(centroid)-Fe-P plane followed by the reassociation of tin would generate **5b**. Based on the equilibrium ratio of **5a**:**5b** (1:2), it can be calculated that **5b** is only minutely energetically favored compared to **5a**, with  $\Delta G = -0.41 \text{ kcal mol}^{-1}$  at 298 K. The greater stability of **5b** compared to **5a** is reproduced by single-point energy calculations (see [Supporting Information](#) page S20) at the DLPNO-CCSD(T)//def2-TZVPP/CPCM(benzene) level of theory, where  $\Delta G$  is computed to be  $-1.7 \text{ kcal mol}^{-1}$  at 298 K.

For the conversion of **1** to **5a,b**, an inverse kinetic isotope effect (KIE) of  $k_{\text{H}}/k_{\text{D}} = 0.68(2)$  was measured by comparing rates for the deuterated ferrostannylene  $\text{Cp}^*(\text{iPr}_2\text{MeP})\text{D}_2\text{Fe-SnDMP}$  (**1-d<sub>2</sub>**) and the corresponding protio-isotopologue (**1**). This suggests a late transition state for the reductive elimination of H<sub>2</sub> by **1**/**1-d<sub>2</sub>** and/or a pre-equilibrium involving an  $\eta^2\text{-H}_2/\text{D}_2$  complex ([Scheme 3](#), steps I and II).<sup>65</sup> The activation parameters for the thermolysis of **1** were measured by an Eyring analysis (340–360 K) to reveal a  $\Delta G^\ddagger_{298 \text{ K}}$  value of  $24.6 \pm 2.0 \text{ kcal mol}^{-1}$  ( $\Delta H^\ddagger = 18.9 \pm 1.5 \text{ kcal mol}^{-1}$ ,  $\Delta S^\ddagger = -18.8 \pm 4.3 \text{ cal mol}^{-1}\text{K}^{-1}$ ).<sup>65</sup> Overall, these data indicate that elimination of H<sub>2</sub> from **1** to produce **A** is rate-determining and that C-H bond activation occurs at a later step. This is further supported by the fact that **5a,b** are formed at ambient temperatures upon chemical reduction of **3**, which does not possess hydride ligands that must be eliminated prior to C-H bond activation.

To probe the possibility of alternative radical-based C-H bond activation mechanisms, the thermolysis of **1** in benzene-*d*<sub>6</sub> was also performed in the presence of 10 equiv of 9,10-dihydroanthracene or 10 equiv of 2,6-di-*tert*-butyl-4-methylphenol. In both cases, the conversion to **5a,b** was unimpeded,

and  $k_{\text{obs}}$  in the presence of these additives was minimally changed (see Supporting Information, Table S3), suggesting that radical and/or H atom transfer pathways are not operative. Also, this reaction is unlikely to be proton-catalyzed, as the kinetic profile was similarly unaffected by the presence of 1 equiv of proton sponge (1,8-bis(dimethylamino)naphthalene). Interestingly, an analogous C–H bond activation is not observed upon thermolysis of the Ru congener of **1**,  $\text{Cp}^*(\text{Pr}_2\text{MeP})(\text{H})_2\text{RuSnDMP}$  (**1**<sub>Ru</sub>). Heating a benzene- $d_6$  solution of **1**<sub>Ru</sub> to 90 °C for several hours resulted in no consumption of the starting material, and no evolution of  $\text{H}_2$  was evident. This difference in reactivity can be attributed in part to the greater reactivity of the hydride ligands in **1**, which are readily eliminated at elevated temperatures.

## CONCLUDING REMARKS

The heterobimetallic Fe–Sn complexes reported here undergo transformations that are strongly influenced by changes in the Fe–Sn bond order. The observed reactions reflect the ability of the tin-based ligand to respond to redox events at iron through geometric changes (e.g., bent vs linear) that affect the number of electrons stored in the Fe–Sn linkage. Perhaps as a result of the low electronegativity of tin, the [SnDMP] ligand engages in substantial electron donation with localization of positive charge in complexes **3** and **4**. As such, [SnDMP] is similar to the nitrosyl ligand in acting as a buffer that accommodates changes in electron density at the metal center.<sup>66,67</sup> In this way, Fe–Sn multiple bonds may enable new pathways to reactive chemical intermediates.

The reactions to produce **5a,b** represent an unusual example of a C–H bond activation mediated by a tin-containing compound. Relevantly, previous reports of aliphatic C–H bond activation involving a low-valent tin center appear to proceed through radical-based intermediates. For example, a mixture of  $[(\text{Me}_3\text{Si})_2\text{N}]_2\text{Sn}$  and phenyl iodide activates alkanes to produce  $[(\text{Me}_3\text{Si})_2\text{N}]_2\text{Sn}(\text{I})(\text{alkyl})$  and benzene via a radical chain mechanism.<sup>68</sup> A more recent report describes C–H bond metathesis in the presence of toluene by  $\text{Ar}_2\text{Sn}$ : ( $\text{Ar}$  = 2,6-bis-(2,6-diisopropylphenyl)phenyl), leading to the formation of  $\text{ArH}$  and 0.5 equiv of  $[\text{Ar}(\text{PhCH}_2)\text{Sn}]_2$ . Freeze-quenched EPR spectra of the mixture formed following photolysis or thermolysis of a solution of  $\text{Ar}_2\text{Sn}$ : shows the presence of a radical consistent with  $[\text{ArSn}\cdot]$ .<sup>69</sup> On the basis of the results described here, the incorporation of transition-metal substituents into low-valent tin compounds represents a new avenue for enabling challenging bond activations via alternate mechanisms and potentially in an intermolecular fashion.<sup>70,71</sup> Current efforts are devoted to developing additional insight into the role of unsaturation at such transition-metal main-group centers in promoting reactivity.

## ASSOCIATED CONTENT

### Supporting Information

The Supporting Information is available free of charge at <https://pubs.acs.org/doi/10.1021/jacs.1c10144>.

Experimental methods, details of syntheses, details of crystallography, EPR and  $^{57}\text{Fe}$  Mössbauer spectroscopy, details of calculations, NMR spectra (PDF)

Cartesian coordinates (XYZ)

## Accession Codes

CCDC 2079318–2079322 contain the supplementary crystallographic data for this paper. These data can be obtained free of charge via [www.ccdc.cam.ac.uk/data\\_request/cif](http://www.ccdc.cam.ac.uk/data_request/cif), or by emailing [data\\_request@ccdc.cam.ac.uk](mailto:data_request@ccdc.cam.ac.uk), or by contacting The Cambridge Crystallographic Data Centre, 12 Union Road, Cambridge CB2 1EZ, UK; fax: + 44 1223 336033.

## AUTHOR INFORMATION

### Corresponding Author

T. Don Tilley – Department of Chemistry, University of California, Berkeley, Berkeley, California 94720, United States; [orcid.org/0000-0002-6671-9099](https://orcid.org/0000-0002-6671-9099); Email: [tdtilley@berkeley.edu](mailto:tdtilley@berkeley.edu)

### Authors

Rex C. Handford – Department of Chemistry, University of California, Berkeley, Berkeley, California 94720, United States; [orcid.org/0000-0002-3693-1697](https://orcid.org/0000-0002-3693-1697)

Mark A. Nesbit – Department of Chemistry, University of California, Davis, Davis, California 95616, United States; [orcid.org/0000-0002-5642-9303](https://orcid.org/0000-0002-5642-9303)

Patrick W. Smith – Department of Chemistry, University of California, Berkeley, Berkeley, California 94720, United States; [orcid.org/0000-0001-5575-4895](https://orcid.org/0000-0001-5575-4895)

R. David Britt – Department of Chemistry, University of California, Davis, Davis, California 95616, United States; [orcid.org/0000-0003-0889-8436](https://orcid.org/0000-0003-0889-8436)

Complete contact information is available at: <https://pubs.acs.org/10.1021/jacs.1c10144>

## Notes

The authors declare no competing financial interest.

## ACKNOWLEDGMENTS

This work was funded by the National Science Foundation under grant no. CHE-1954808. R.C.H. thanks the NSERC of Canada for a PGS-D fellowship. This research used the resources of the Advanced Light Source, which is a DOE Office of Science User Facility under contract no. DE-AC02-05CH11231. We thank Dr. Simon J. Teat for his assistance with X-ray diffraction experiments. Computations were performed using the Tiger cluster at the Molecular Graphics and Computation Facility (MGCF) of the University of California, Berkeley, which is supported by the National Institutes of Health under grant no. NIH S10OD023532, and we thank Dr. Kathleen Durkin and Dr. Dave Small for their advice and expertise on computations. NMR spectra were collected at the College of Chemistry NMR facility, at the University of California, Berkeley, which is supported in part by the National Institutes of Health under grant no. S10OD024998; we thank Dr. Hasan Celic and Dr. Alicia Lund for advice and assistance with NMR spectroscopy. Dr. Benjamin A. Suslick, Dr. Pablo Rios, Dr. Addison N. Desnoyer, T. Alex Wheeler, and Dr. Stefan A. Küenzi are gratefully acknowledged for their helpful insights.

## REFERENCES

- Balázs, G.; Gregoriades, L. J.; Scheer, M. Triple Bonds between Transition Metals and the Heavier Elements of Groups 14 and 15. *Organometallics* **2007**, *26*, 3058–3075.
- Fischer, R. C.; Power, P. P.  $\pi$ -Bonding and the Lone Pair Effect in Multiple Bonds Involving Heavier Main Group Elements:



Developments in the New Millennium. *Chem. Rev.* **2010**, *110*, 3877–3923.

(3) Less, R. J.; Wright, D. S. Group 14 Metal-Metal Bonds. In *Molecular Metal-Metal Bonds: Compounds, Synthesis, Properties*; Liddle, S. T., Ed.; Wiley-VCH Verlag GmbH & Co. KGaA: Weinheim, Germany, 2015; pp 485–517.

(4) Somerville, R. J.; Campos, J. Cooperativity in Transition Metal Tetraylene Complexes. *Eur. J. Inorg. Chem.* **2021**, *2021*, 3488–3498.

(5) Waterman, R.; Hayes, P. G.; Tilley, T. D. Synthetic Development and Chemical Reactivity of Transition-Metal Silylene Complexes. *Acc. Chem. Res.* **2007**, *40*, 712–719.

(6) Hashimoto, H.; Tobita, H. Recent Advances in the Chemistry of Transition Metal-Silicon/Germanium Triple-Bonded Complexes. *Coord. Chem. Rev.* **2018**, *355*, 362–379.

(7) Wang, Z.; Hu, H.; Szentpály, L.; Stoll, H.; Fritzsche, S.; Pyykkö, P.; Schwarz, W. H. E.; Li, J. Understanding the Uniqueness of 2p Elements in Periodic Tables. *Chem. - Eur. J.* **2020**, *26*, 15558–15564.

(8) Jutzi, P. New Element-Carbon (p-p) $\pi$  Bonds. *Angew. Chem., Int. Ed. Engl.* **1975**, *14*, 232–245.

(9) West, R. Multiple Bonds to Silicon: 20 Years Later. *Polyhedron* **2002**, *21*, 467–472.

(10) Power, P. P. An Update on Multiple Bonding between Heavier Main Group Elements: The Importance of Pauli Repulsion, Charge-Shift Character, and London Dispersion Force Effects. *Organometallics* **2020**, *39*, 4127–4138.

(11) Lipke, M. C.; Liberman-Martin, A. L.; Tilley, T. D. Electrophilic Activation of Silicon-Hydrogen Bonds in Catalytic Hydrosilations. *Angew. Chem., Int. Ed.* **2017**, *56*, 2260–2294.

(12) Hayes, P. G.; Waterman, R.; Glaser, P. B.; Tilley, T. D. Synthesis, Structure, and Reactivity of Neutral Hydrogen-Substituted Ruthenium Silylene and Germylene Complexes. *Organometallics* **2009**, *28*, 5082–5089.

(13) Glaser, P. B.; Tilley, T. D. Catalytic Hydrosilylation of Alkenes by a Ruthenium Silylene Complex. Evidence for a New Hydro-silylation Mechanism. *J. Am. Chem. Soc.* **2003**, *125*, 13640–13641.

(14) Fasulo, M. E.; Lipke, M. C.; Tilley, T. D. Structural and Mechanistic Investigation of a Cationic Hydrogen-Substituted Ruthenium Silylene Catalyst for Alkene Hydrosilation. *Chem. Sci.* **2013**, *4*, 3882–3887.

(15) Filippou, A. C.; Chernov, O.; Schnakenburg, G. Metal-Silicon Triple Bonds: Nucleophilic Addition and Redox Reactions of the Silyldiyne Complex  $[\text{Cp}(\text{CO})_2\text{Mo}\equiv\text{Si-R}]$ . *Angew. Chem., Int. Ed.* **2011**, *50*, 1122–1126.

(16) Widemann, M.; Eichele, K.; Schubert, H.; Sindlinger, C. P.; Klenner, S.; Pöttgen, R.; Wesemann, L. Synthesis and Hydrogenation of Heavy Homologues of Rhodium Carbynes:  $[(\text{Me}_3\text{P})_2(\text{Ph}_3\text{P})\text{Rh}\equiv\text{E-Ar}^*]$  (E = Sn, Pb). *Angew. Chem., Int. Ed.* **2021**, *60*, 5882–5889.

(17) Hayes, P. G.; Gribble, C. W.; Waterman, R.; Tilley, T. D. A Hydrogen-Substituted Osmium Stannylene Complex: Isomerization to a Metallostannylene Complex via an Unusual  $\alpha$ -Hydrogen Migration from Tin to Osmium. *J. Am. Chem. Soc.* **2009**, *131*, 4606–4607.

(18) Liu, H.-J.; Ziegler, M. S.; Tilley, T. D. The Ruthenostannylene Complex  $[\text{Cp}^*(\text{IXy})\text{H}_2\text{Ru-Sn-Trip}]$ : Providing Access to Unusual Ru-Sn Bonded Stanna-Imine, Stannene, and Ketenylstannyl Complexes. *Angew. Chem., Int. Ed.* **2015**, *54*, 6622–6626.

(19) Smith, P. W.; Handford, R. C.; Tilley, T. D. Heavy Tetrel Complexes of Ru Featuring Ru = E(R)X and Ru-E-R (E = Sn, Pb) Linkages. *Organometallics* **2019**, *38*, 4060–4065.

(20) Pu, L.; Twamley, B.; Haubrich, S. T.; Olmstead, M. M.; Mork, B. V.; Simons, R. S.; Power, P. P. Triple Bonding to Germanium: Characterization of the Transition Metal Germynes  $(\eta^5\text{-C}_5\text{H}_5)(\text{CO})_2\text{M}:\text{Ge-C}_6\text{H}_3\text{-2,6-Mes}_2$  (M = Mo, W; Mes =  $-\text{C}_6\text{H}_3\text{-2,4,6-Me}_3$ ) and  $(\eta^5\text{-C}_5\text{H}_5)(\text{CO})_2\text{M}:\text{Ge-C}_6\text{H}_3\text{-2,6-Trip}_2$  (M = Cr, Mo, W; Trip =  $-\text{C}_6\text{H}_2\text{-2,4,6-}^i\text{Pr}_3$ ) and the Related Single Bonded Metallogermynes  $(\eta^5\text{-C}_5\text{H}_5)(\text{CO})_3\text{M}:\text{Ge-C}_6\text{H}_3\text{-2,6-Trip}_2$  (M = Cr, W). *J. Am. Chem. Soc.* **2000**, *122*, 650–656.

(21) Hayes, P. G.; Xu, Z.; Beddie, C.; Keith, J. M.; Hall, M. B.; Tilley, T. D. The Osmium-Silicon Triple Bond: Synthesis, Character-

ization, and Reactivity of an Osmium Silylyne Complex. *J. Am. Chem. Soc.* **2013**, *135*, 11780–11783.

(22) Inomata, K.; Watanabe, T.; Miyazaki, Y.; Tobita, H. Insertion of a Cationic Metallogermylene into E-H Bonds (E = H, B, Si). *J. Am. Chem. Soc.* **2015**, *137*, 11935–11937.

(23) Holland, P. L. Distinctive Reaction Pathways at Base Metals in High-Spin Organometallic Catalysts. *Acc. Chem. Res.* **2015**, *48*, 1696–1702.

(24) Bellows, S. M.; Cundari, T. R.; Holland, P. L. Spin Crossover during  $\beta$ -Hydride Elimination in High-Spin Iron(II)- and Cobalt(II)-Alkyl Complexes. *Organometallics* **2013**, *32*, 4741–4751.

(25) Fürstner, A. Iron Catalysis in Organic Synthesis: A Critical Assessment of What It Takes To Make This Base Metal a Multitasking Champion. *ACS Cent. Sci.* **2016**, *2*, 778–789.

(26) Detrich, J. L.; Reinaud, O. M.; Rheingold, A. L.; Theopold, K. H. Can Spin State Change Slow Organometallic Reactions? *J. Am. Chem. Soc.* **1995**, *117*, 11745–11748.

(27) Carreón-Macedo, J.-L.; Harvey, J. N. Do Spin State Changes Matter in Organometallic Chemistry? A Computational Study. *J. Am. Chem. Soc.* **2004**, *126*, 5789–5797.

(28) Smith, P. W.; Tilley, T. D. Base-Free Iron Hydrosilylene Complexes via an  $\alpha$ -Hydride Migration That Induces Spin Pairing. *J. Am. Chem. Soc.* **2018**, *140*, 3880–3883.

(29) Smith, P. W.; Dong, Y.; Tilley, T. D. Efficient and Selective Alkene Hydrosilation Promoted by Weak, Double Si-H Activation at an Iron Center. *Chem. Sci.* **2020**, *11*, 7070–7075.

(30) Jiang, Y.; Schirmer, B.; Blacque, O.; Fox, T.; Grimme, S.; Berke, H. The “Catalytic Nitrosyl Effect”: NO Bending Boosting the Efficiency of Rhenium Based Alkene Hydrogenations. *J. Am. Chem. Soc.* **2013**, *135*, 4088–4102.

(31) Jiang, Y.; Huang, W.; Schmalle, H. W.; Blacque, O.; Fox, T.; Berke, H. Structural Evidence for Lewis Acid Triggered Nitrosyl Bending in Rhenium(-I) Chloro Catalysts for Alkene Hydrogenation Reactions: Rhenium Chloro Catalysts in Alkene Hydrogenation Reactions. *Eur. J. Inorg. Chem.* **2014**, *2014*, 140–147.

(32) Richter-Addo, G. B.; Legzdins, P. *Metal Nitrosyls*; Oxford University Press: Oxford, England, 1992.

(33) Liu, H.-J.; Guihaumé, J.; Davin, T.; Raynaud, C.; Eisenstein, O.; Tilley, T. D. 1,2-Hydrogen Migration to a Saturated Ruthenium Complex via Reversal of Electronic Properties for Tin in a Stannylene-to-Metallostannylene Conversion. *J. Am. Chem. Soc.* **2014**, *136*, 13991–13994.

(34) A search of Sn-H bonds in the *Cambridge Structural Database* (version 5.41, update 3) indicates a mean bond distance of 1.731 Å.

(35) Güttlich, P. Fifty Years of Mössbauer Spectroscopy in Solid State Research - Remarkable Achievements, Future Perspectives. *Z. Anorg. Allg. Chem.* **2012**, *638*, 15–43.

(36) Parkin, G. Valence, Oxidation Number, and Formal Charge: Three Related but Fundamentally Different Concepts. *J. Chem. Educ.* **2006**, *83*, 791–799.

(37) Wolczanski, P. T. Flipping the Oxidation State Formalism: Charge Distribution in Organometallic Complexes As Reported by Carbon Monoxide. *Organometallics* **2017**, *36*, 622–631.

(38) Eichler, B. E.; Phillips, A. D.; Haubrich, S. T.; Mork, B. V.; Power, P. P. Synthesis, Structures, and Spectroscopy of the Metallostannylenes  $(\eta^5\text{-C}_5\text{H}_5)(\text{CO})_3\text{M}-\text{Sn-C}_6\text{H}_3\text{-2,6-Ar}_2$  (M = Cr, Mo, W; Ar =  $\text{C}_6\text{H}_2\text{-2,4,6-Me}_3$ ,  $\text{C}_6\text{H}_2\text{-2,4,6-Pr}_3$ ). *Organometallics* **2002**, *21*, 5622–5627.

(39) Lei, H.; Guo, J.-D.; Fetting, J. C.; Nagase, S.; Power, P. P. Synthesis, Characterization, and CO Elimination of Ferrio-Substituted Two-Coordinate Germynes and Stannylenes. *Organometallics* **2011**, *30*, 6316–6322.

(40) Filippou, A. C.; Ghana, P.; Chakraborty, U.; Schnakenburg, G. Manganese-Tin Triple Bonds: A New Synthetic Route to the Manganese Stannylidyne Complex Cation *Trans*- $[\text{H}(\text{Dmpe})_2\text{Mn}\equiv\text{Sn}(\text{C}_6\text{H}_3\text{-2,6-Mes}_2)]^+$  (Dmpe =  $\text{Me}_2\text{PCH}_2\text{CH}_2\text{PMe}_2$ , Mes = 2,4,6-Trimethylphenyl). *J. Am. Chem. Soc.* **2013**, *135*, 11525–11528.

(41) Nesbit, M. A.; Oyala, P. H.; Peters, J. C. Characterization of the Earliest Intermediate of Fe-N<sub>2</sub> Protonation: CW and Pulse EPR

Detection of an Fe-NNH Species and Its Evolution to Fe-NNH<sub>2</sub><sup>+</sup>. *J. Am. Chem. Soc.* **2019**, *141*, 8116–8127.

(42) Gilbert-Wilson, R.; Field, L. D.; Colbran, S. B.; Bhadbhade, M. M. Low Oxidation State Iron(0), Iron(I), and Ruthenium(0) Dinitrogen Complexes with a Very Bulky Neutral Phosphine Ligand. *Inorg. Chem.* **2013**, *52*, 3043–3053.

(43) Therien, M. J.; Trogler, W. C. Tricarbonylbis(Phosphine)Iron-(I) Cation Radicals. A Spectroscopic and Theoretical Study. *J. Am. Chem. Soc.* **1986**, *108*, 3697–3702.

(44) Karnahl, M.; Tschierlei, S.; Erdem, Ö. F.; Pullen, S.; Santoni, M.-P.; Reijerse, E. J.; Lubitz, W.; Ott, S. Mixed-Valence [Fe<sup>I</sup>Fe<sup>II</sup>] Hydrogenase Active Site Model Complexes Stabilized by a Bidentate Carborane Bis-Phosphine Ligand. *Dalton Trans.* **2012**, *41*, 12468–12477.

(45) Sekiguchi, A.; Fukawa, T.; Lee, V. Ya.; Nakamoto, M. Tin-Centered Radical and Cation: Stable and Free. *J. Am. Chem. Soc.* **2003**, *125*, 9250–9251.

(46) Power, P. P. Persistent and Stable Radicals of the Heavier Main Group Elements and Related Species. *Chem. Rev.* **2003**, *103*, 789–809.

(47) Wang, S.; Tao, L.; Stich, T. A.; Olmstead, M. M.; Britt, R. D.; Power, P. P. Insertion of a Transient Tin Nitride into Carbon-Carbon and Boron-Carbon Bonds. *Inorg. Chem.* **2017**, *56*, 14596–14604.

(48) Lai, T. Y.; Tao, L.; Britt, R. D.; Power, P. P. Reversible Sn-Sn Triple Bond Dissociation in a Distannyne: Support for Charge-Shift Bonding Character. *J. Am. Chem. Soc.* **2019**, *141*, 12527–12530.

(49) Watts, G. B.; Griller, D.; Ingold, K. U. Kinetic Applications of Electron Paramagnetic Resonance Spectroscopy. VIII. Tetraalkoxyphosphoranyl Radicals. *J. Am. Chem. Soc.* **1972**, *94*, 8784–8789.

(50) Griller, D.; Roberts, B. P.; Davies, A. G.; Ingold, K. U. Kinetic Applications of Electron Paramagnetic Resonance Spectroscopy. XII. Self-Reactions of Some Phosphorus Centered Radicals. *J. Am. Chem. Soc.* **1974**, *96*, 554–556.

(51) Davies, A. G.; Griller, D.; Roberts, B. P. Electron Spin Resonance Study of Dialkoxyposphonyl Radicals, (RO)<sub>2</sub>PO. *J. Am. Chem. Soc.* **1972**, *94*, 1782–1783.

(52) Dennis, R. W.; Roberts, B. P. An ESR Study on the Reactions of T-Butoxyl Radicals with Aminophosphines. *J. Organomet. Chem.* **1972**, *43*, C2–C4.

(53) Gütlich, P.; Schröder, C.; Schünemann, V. Mössbauer Spectroscopy—an Indispensable Tool in Solid State Research. *SpectroscopyEurope* **2012**, *24*, 21–31.

(54) Pápai, M.; Vankó, G. On Predicting Mössbauer Parameters of Iron-Containing Molecules with Density-Functional Theory. *J. Chem. Theory Comput.* **2013**, *9*, 5004–5020.

(55) Lin, Y.-S.; Li, G.-D.; Mao, S.-P.; Chai, J.-D. Long-Range Corrected Hybrid Density Functionals with Improved Dispersion Corrections. *J. Chem. Theory Comput.* **2013**, *9*, 263–272.

(56) Weigend, F.; Ahlrichs, R. Balanced Basis Sets of Split Valence, Triple Zeta Valence and Quadruple Zeta Valence Quality for H to Rn: Design and Assessment of Accuracy. *Phys. Chem. Chem. Phys.* **2005**, *7*, 3297–3305.

(57) Dryden, N. H.; Legzdins, P.; Einstein, F. W. B.; Jones, R. H. Synthesis and Characterization of (η<sup>5</sup>-C<sub>5</sub>Me<sub>5</sub>)W(NO)I<sub>2</sub>, a Monomeric, Formally 16-Electron Complex. *Can. J. Chem.* **1988**, *66*, 2100–2103.

(58) Hayton, T. W.; Legzdins, P.; Sharp, W. B. Coordination and Organometallic Chemistry of Metal-NO Complexes. *Chem. Rev.* **2002**, *102*, 935–991.

(59) Wiberg, K. B. Application of the Pople-Santry-Segal CNDO Method to the Cyclopropylcarbanyl and Cyclobutyl Cation and to Bicyclobutane. *Tetrahedron* **1968**, *24*, 1083–1096.

(60) Cancès, E.; Mennucci, B.; Tomasi, J. A New Integral Equation Formalism for the Polarizable Continuum Model: Theoretical Background and Applications to Isotropic and Anisotropic Dielectrics. *J. Chem. Phys.* **1997**, *107*, 3032–3041.

(61) Deul, R.; Rosenzweig, S.; Franck, E. U. The Dielectric Constant and Density of Benzene to 400 °C and 3000 bar. *Berichte Bunsenges. Für Phys. Chem.* **1991**, *95*, 515–519.

(62) Behn, A.; Zimmerman, P. M.; Bell, A. T.; Head-Gordon, M. Efficient Exploration of Reaction Paths via a Freezing String Method. *J. Chem. Phys.* **2011**, *135*, 224108–1.

(63) Liakos, D. G.; Guo, Y.; Neese, F. Comprehensive Benchmark Results for the Domain Based Local Pair Natural Orbital Coupled Cluster Method (DLPNO-CCSD(T)) for Closed- and Open-Shell Systems. *J. Phys. Chem. A* **2020**, *124*, 90–100.

(64) Barone, V.; Cossi, M. Quantum Calculation of Molecular Energies and Energy Gradients in Solution by a Conductor Solvent Model. *J. Phys. Chem. A* **1998**, *102*, 1995–2001.

(65) Packett, D. L.; Trogler, W. C. Kinetics of Cis-Trans Isomerization and Reductive Elimination in Dihydridobis-(Trimethylphosphine)Platinum(II). *Inorg. Chem.* **1988**, *27*, 1768–1775.

(66) Chalkley, M. J.; Peters, J. C. A Triad of Highly Reduced, Linear Iron Nitrosyl Complexes: {FeNO}<sup>8–10</sup>. *Angew. Chem., Int. Ed.* **2016**, *55*, 11995–11998.

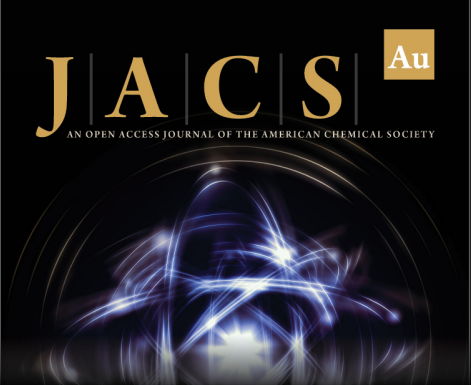
(67) Dong, H. T.; Chalkley, M. J.; Oyala, P. H.; Zhao, J.; Alp, E. E.; Hu, M. Y.; Peters, J. C.; Lehnert, N. Exploring the Limits of Dative Boratrane Bonding: Iron as a Strong Lewis Base in Low-Valent Non-Heme Iron-Nitrosyl Complexes. *Inorg. Chem.* **2020**, *59*, 14967–14982.

(68) Bartolin, J. M.; Kavara, A.; Kampf, J.; Banaszak Holl, M. M. Tin-Mediated CH Activation and Cross-Coupling in a Single Flask. *Organometallics* **2006**, *25*, 4738–4740.


(69) Lai, T. Y.; Fettingner, J. C.; Power, P. P. Facile C-H Bond Metathesis Mediated by a Stannylene. *J. Am. Chem. Soc.* **2018**, *140*, 5674–5677.

(70) Dorantes, M. J.; Moore, J. T.; Bill, E.; Mienert, B.; Lu, C. C. Bimetallic Iron-Tin Catalyst for N<sub>2</sub> to NH<sub>3</sub> and a Silyldiazenido Model Intermediate. *Chem. Commun.* **2020**, *56*, 11030–11033.


(71) Mankad, N. P. Selectivity Effects in Bimetallic Catalysis. *Chem.-Eur. J.* **2016**, *22*, 5822–5829.




**JACS** Au  
AN OPEN ACCESS JOURNAL OF THE AMERICAN CHEMICAL SOCIETY



Editor-in-Chief  
**Prof. Christopher W. Jones**  
Georgia Institute of Technology, USA

**Open for Submissions** 

pubs.acs.org/jacsau  ACS Publications  
Most Trusted. Most Cited. Most Read.